Corneal surface reconstruction algorithm using Zernike polynomial representation: improvements

Jason Turuwhenua

Bioengineering Institute, Faculty of Engineering, University of Auckland, New Zealand

Received February 10, 2006; revised October 11, 2006; accepted October 28, 2006; posted December 18, 2006 (Doc. ID 67432); published May 9, 2007

Recently Sicam *et al.* [J. Opt. Soc. Am. A **21**, 1300 (2004)] presented a new corneal reconstruction algorithm for estimating corneal sag by Zernike polynomials. An equivalent but simpler derivation of the model equations is presented. The algorithm is tested on a sphere, a conic, and a toric. These tests reveal significant height errors that accrue with distance from the corneal apex. Additional postprocessing steps are introduced to circumvent these errors. A consistent and significant reduction in height errors is observed across the test surfaces. Finally, Sicam *et al.* used the conic p-value p as a measure of algorithm efficacy. Further investigation shows that the finite Zernike representation affected the reported results. The p-value should therefore be used with caution as an efficacy measure.

OCIS codes: 170.4460, 170.3890.

1. INTRODUCTION

Corneal topography has had significant impact on the screening and planning of refractive surgical procedures.[1] It is a standard modality in the preoperative examination for refractive surgery, and the postoperative assessment of surgical complications.[1] The state of the art in corneal topography is Placido-disk videokeratography.[2] That approach projects a source consisting of illuminated concentric rings to a CCD camera after reflection in the anterior cornea. The correspondence between measured CCD points and points on the Placido disk leads to a reconstruction of corneal shape.

Actually, a given measured CCD point cannot be associated with a *unique* point on a *continuous* Placido ring.[2,3] While it may be possible to identify the ring of the measured CCD point with the corresponding ring on the Placido cone, the angular distance between a given CCD point and source point cannot be determined from an image of Placido rings alone. The standard work around in designing reconstruction algorithms has been to assume that corneal tilt (slope in the azimuthal direction) is negligible. Then rays are assumed to lie in the meridional plane, and a unique correspondence between a point on the CCD plane and the Placido cone can be made. At the same time that assumption introduces the skew-ray error,[3,4] which leads to height reconstruction errors due to the presence of corneal tilt in real corneas. Even so, Klein[4] showed that it was possible to estimate corneal tilt without additional cues. This estimate of corneal tilt was used to account for skew rays and produced height errors well below micrometer level. In addition, Halstead *et al.* described a Placido-based method using a nonlinear optimization that appeared to work well for nonsymmetric corneas.[5]

Methods that avoid the skew-ray error by using non-Placido source patterns such as checkerboards have been reported.[6,7] Recently, Sicam *et al.* (2004) described a method suitable for use with discrete source points, combined with an iterative least-squares method based on Zernike polynomials.[8] In fact, the iterative least-squares approach had been described previously for a Placido-disk-based method using tensor product B-spline surfaces.[9] A clear departure of the Sicam *et al.* (2004) approach (to be referred to as the Ref. 8 approach), was that model equations were derived that produced (Zernike) coefficients corresponding directly to *corneal sagittal depth* or *corneal sag*.

The idea that discrete points might address skew-ray error problems has intuitive appeal. Nevertheless, the conditions under which discrete sources may provide a better solution than ring sources say, are not entirely clear. The literature has not yet provided (to the knowledge of the author) a direct comparison of these approaches. Indeed, the concern of Ref. 8 was to present the details of a method suitable for use with discrete sources, rather than to compare alternate approaches. Moreover, the efficacy of any particular method depends on a number of issues such as: the order and type of basis functions used, sampling, and noise response, as well as the ability to localize source points in images. These are issues that should be analyzed in detail if the relative merits of alternative approaches are to be fully appreciated.

This paper does not address the issue of the relative merits of discrete points versus Placido rings, but it does seek to make some progress toward an answer. Instead, the present paper provides an analysis of the Ref. 8 algorithm, and seeks to show that room for further improvement exists. First, an alternate but entirely equivalent derivation of the key relationship between the corneal surface and the rays used to probe that surface is presented. While the final recasted equations are the same as those presented in the original paper, the rederivation

provides additional insight into the sources of potential reconstruction error. An improvement step is then suggested. It is proposed that an additional Zernike fitting step be added in postprocessing (to surface intersection data), in order to produce a more accurate estimate of corneal *sag*. The use of the additional step is supported by subsequent tests applied to a sphere, a conic surface, and a toric surface. These results suggest that Zernike polynomials combined with a discrete source array are able to recover these surfaces with good accuracy. Further tests on a model of radial keratotomy (RK) agree with results presented in the original Ref. 8 analysis. However, there is no significant improvement upon those results. The possible reasons for that observation are outlined.

In Ref. 8 the conic p-value p and the central radius R were determined from the reconstructed Zernike coefficients (for a spherical and conic surface). A reconstructed p-value that was close to the true p-value (i.e., of the exactly known surface) was used to indicate good height reconstruction. However, a more detailed analysis reveals that errors in both R and p were due mainly to the order of the Zernike representation rather than height errors. That finding suggests that p-value should be used with caution if it is used as a measure of efficacy.

2. THEORY

A. Recasting the Sicam *et al.* Algorithm

This section reviews the least-squares approach to corneal topography implemented in Ref. 8. It is noted that this algorithm was developed assuming discrete source points, but steps[9] have been used previously, that were used to account for continuous ring sources. These additional steps (as they apply to this algorithm) will be described briefly in Section 5. Therefore, this method can be regarded as suitable for use in general corneal topography (i.e., regardless of source continuity).

The current derivation differs from that in Ref. 8, in that the corneal intersection depth (z_p) is derived in a new way. An additional postprocessing step is also suggested in the next section, which it is proposed, will produce an improved estimate of corneal sag. Otherwise, the derivation is similar to an approach originally used by Halstead *et al.*[9] Explicit equations will be derived here for convenience. To be consistent with the Ref. 8 derivation, Figs. 1 and 2 show adaptations of Figs. 3 and 4 of the Ref. 8 paper. The same labeling has been used, but the figures differ to emphasize the features of the new derivation. To further emphasize the correspondence between the two derivations, it will be pointed out when equations that appeared in the Ref. 8 exposition are identical.

Consider then Fig. 1, showing a measured CCD point $C(u,v,-2OA)$ [i.e., with CCD coordinates (u,v)] sitting an axial distance OA to the left of the nodal point. (It is assumed here that $OA=OB$.) The corneal sag is z (the length DF in Fig. 2), which sits at the surface point $F(-u,-v,z)$. The point where the incident ray strikes the corneal surface is denoted $P(x_p,y_p,z_p)$. The points $F(-u,-v,z)$ and $P(x_p,y_p,z_p)$ are related by the *intersection equations* [Eqs. (8)–(10) of Ref. 8]:

$$x_p = -u - \left(\frac{u}{OA}\right) z_p, \tag{1}$$

$$y_p = -v - \left(\frac{v}{OA}\right) z_p, \tag{2}$$

$$z_p = z(-u,-v)\left(1 + \frac{u^2+v^2}{(OA)(AR)}\right), \tag{3}$$

where the corneal sag $z(-u,-v)$ is given by the Zernike sum

$$z(-u,-v) = \sum c_n^m (Z_n^m(-u,-v) - Z_n^m(0,0)), \tag{4}$$

and the set of coefficients c_n^m thereby represent the corneal sag. The symbol Z_n^m represents the Zernike terms

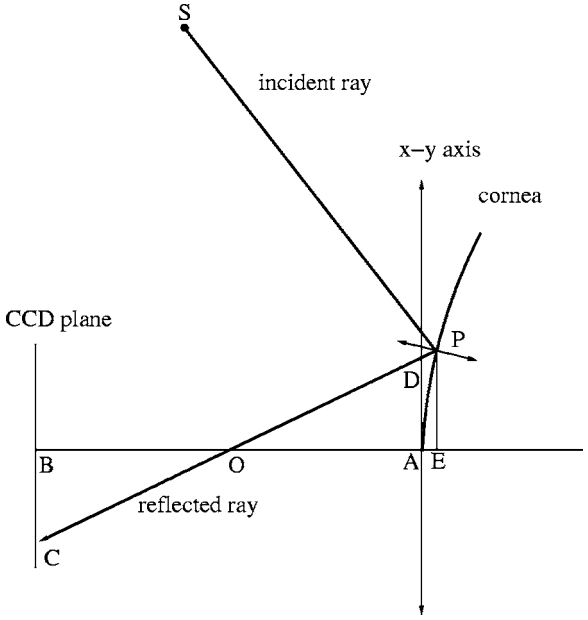

Fig. 1. Overall setup used to recover corneal shape. A ray from a source point S reflects at the corneal surface P, passes through the nodal point O to the CCD plane. The correspondence between a measured point C on the CCD plane and a source point S allows a reconstruction of corneal shape.

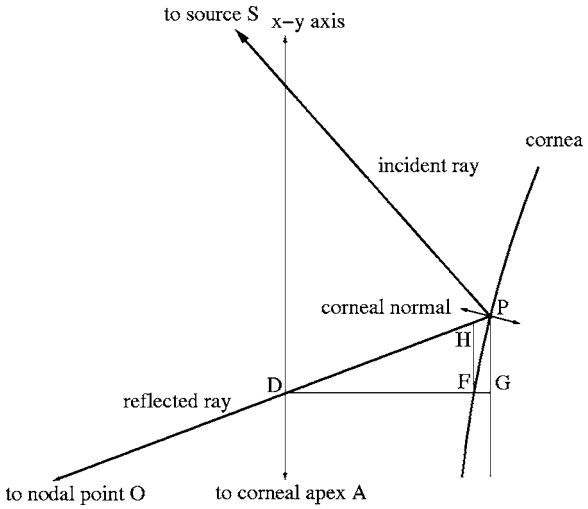

Fig. 2. Closer view of the region where the ray strikes the corneal surface. The distance $z=DF$ is the corneal sag. This point is to be determined from the nearby ray that passes through D and strikes the surface at intersection point P.

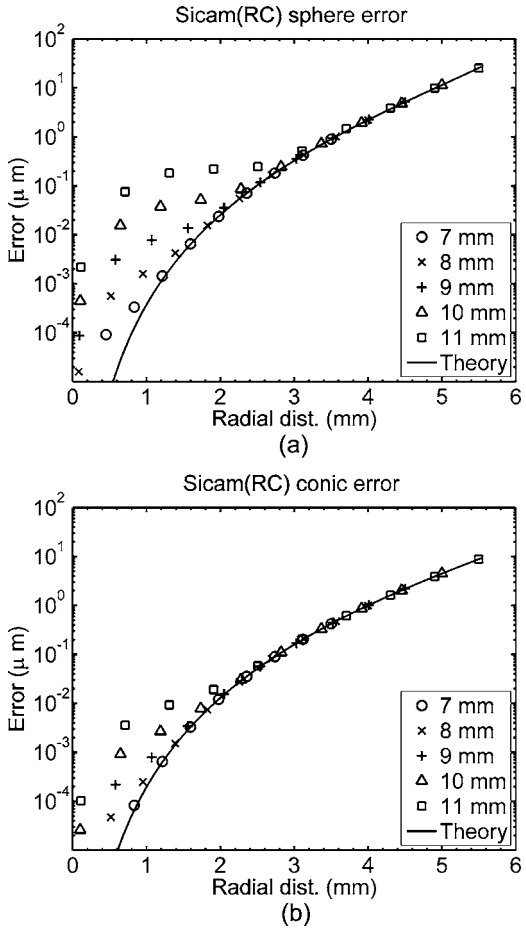

Fig. 3. Reconstruction results for the Sicam (RC) method applied to (a) a sphere ($R=7$ mm) and (b) a conic ($R=7.87$, $p=0.82$). The discrete points show error profiles at each pupil setting (7 to 11 mm). The continuous lines show predicted deviation, that is, the predicted error incurred by the Sicam (RC) method.

where the $Z_n^m(0,0)$ term sets corneal sag to 0 at the corneal apex. In this paper, the naming conventions of Ref. 10 have been adopted.

Now Eqs. (1) and (2) result from using the fact that *OEP* and *OBC* are similar. On the other hand, Eq. (3) is an approximate equation to be determined whereupon the meaning of the constant *AR* will be clarified. To that end, denote the radial distance *AD* by ρ, the distance *GP* by $\Delta\rho'$, and length *FH* by $\Delta\rho$. Approximate the point z_p by the first-order Taylor expansion of z about ρ,

$$z_p \approx z + z'(\rho)\Delta\rho'. \tag{5}$$

A conic cornea can be represented by the equation

$$\rho^2 - 2Rz + pz^2 = 0, \tag{6}$$

where R is the central radius of curvature, and p is the conic p-value.[11] Expanding the corneal sag z to first order gives

$$z = \frac{\rho^2}{2\mathrm{R}}, \tag{7}$$

where R is the radius of the central cornea. This becomes

$$z'(\rho) = \frac{\rho}{R} \tag{8}$$

upon differentiation. From Figs. 1 and 2, triangles *OAD* and *DFH* are similar, so

$$\Delta\rho = \frac{z\rho}{OA}. \tag{9}$$

Assume now that

$$\Delta\rho' \approx \Delta\rho. \tag{10}$$

We substitute Eq. (8) for $z'(\rho)$ in Eq. (5) and eliminate $\Delta\rho'$ in Eq. (5) by Eq. (9) [under the assumption of Eq. (10)]. Replacing the resulting ρ^2 term with $\rho^2=u^2+v^2$ gives Eq. (3) as required.

This derivation of Eqs. (1)–(3) is an alternate route to that taken from Ref. 8, and appears to be a more straightforward approach than originally presented. A useful feature of this new derivation is that it is simple to identify the sources of approximation errors in Eq. (3), namely, the first-order approximation of Eq. (5), the assumption that $\Delta\rho' \approx \Delta\rho$, and the assumption that the cornea is parabolic (to first order). Height errors will arise if the corneal sur-

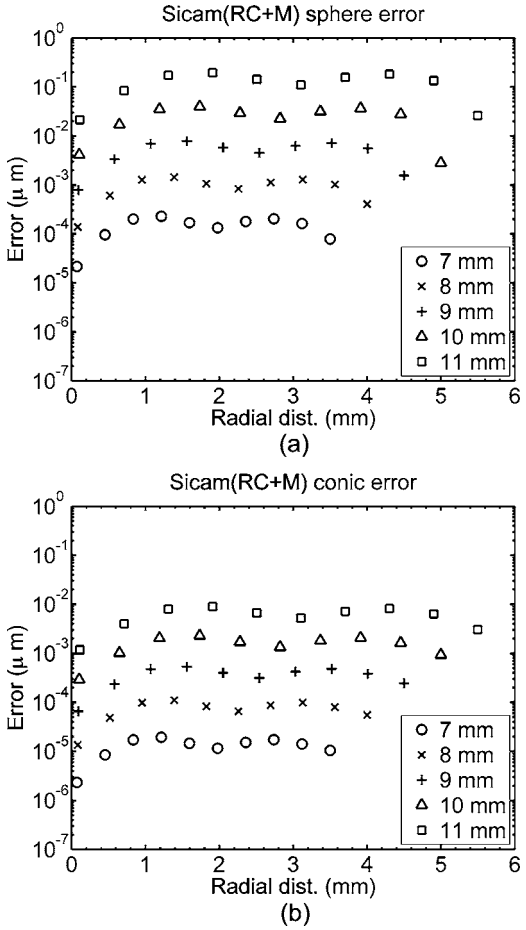

Fig. 4. Reconstruction results for the Sicam (RC+M) method applied to (a) a sphere ($R=7$ mm) and (b) a conic ($R=7.87$, $p=0.82$). The discrete points show error profiles at each pupil setting (7 to 11 mm). Note the large reductions in error after the improved method has been applied.

face departs from these assumptions. While the use of assumptions is potentially undesirable, the resulting approximations yield multiple equations that are *linear* in c_n^m, and therefore are amenable to a simple linear least-squares estimation as will be seen.

Note also at this point, that this derivation sets $AR=R$ (i.e., the central radius of curvature). Equation (13) of Ref. 8 sets $AR=R/a$ (i.e., the central corneal radius normalized by the Zernike aperture radius a). This choice requires that all coordinates be scaled by $1/a$, otherwise Eq. (3) of the present paper [Eq. (8) of Ref. 8] would be dimensionally inconsistent. The present work has used unnormalized coordinates, and therefore normalization factors do not appear.

The formulation of the remaining equations follows in a manner similar to that described by Halstead *et al.* previously.[9] The approach is not new, but the steps have been included to complete the derivation of the original Ref. 8 method. The law of reflection states that the corneal normal n will bisect the incident and reflected rays. Choose then, the particular bisecting vector

$$n = -\frac{\hat{i}+\hat{r}}{(\hat{i}+\hat{r})_z}, \tag{11}$$

where the denominator normalizes the z component of the normal vector to -1. (This is the same as Eq. (19) of Ref. 8, except the normalization used here differs.) The unit incident ray $\hat{i}$ is given by

$$\hat{i} = \frac{S-P}{|S-P|}, \tag{12}$$

and $\hat{r}$ is the unit reflected ray

$$\hat{r} = \frac{C-O}{|C-O|}, \tag{13}$$

which follows from geometry using $S=(x_s,y_s,z_s)$, $P=(x_p,y_p,z_p)$, and $O=(0,0,-OA)$. The reflected ray depends on constants C and O, and consequently will be constant itself. The incident ray depends on P and therefore will depend on the variable Zernike coefficients. At the same time, the tangent *vectors* $\partial P/\partial u$ and $\partial P/\partial v$ to the corneal surface P define the normal $n=(n_x,n_y,-1)$ by

$$n \cdot \frac{\partial P}{\partial u} = 0, \tag{14}$$

$$n \cdot \frac{\partial P}{\partial v} = 0. \tag{15}$$

The law of reflection is satisfied (and hence the solution is determined) when c_n^m are found such that n [determined by Eq. (11)] and the corresponding tangent vectors ($\partial P/\partial u$, $\partial P/\partial v$) satisfy Eqs. (14) and (15). To solve these equations, an iterative solution was proposed.[8,9] Starting with an *estimate* of P determine the n that bisects the incident and reflected rays [Eqs. (11)–(13)]. Then fit a new surface to these *required* n. To do that fitting, enter these n values in Eqs. (14) and (15), yielding two equations in the new and unknown c_n^m. From multiple measurements, form a system of linear equations and solve for c_n^m by linear least squares. To be precise, Appendix A shows that Eqs. (14) and (15) become

$$n_x = \sum_{m,n} c_n^m U_n^m, \tag{16}$$

$$n_y = \sum_{m,n} c_n^m V_n^m, \tag{17}$$

where

$$U_n^m = -\left(1+\frac{n_y v + n_x u}{OA}\right)\frac{\partial \gamma_n^m}{\partial u} - \frac{n_x}{OA}\gamma_n^m, \tag{18}$$

$$V_n^m = -\left(1+\frac{n_y v + n_x u}{OA}\right)\frac{\partial \gamma_n^m}{\partial v} - \frac{n_y}{OA}\gamma_n^m, \tag{19}$$

$$\gamma_n^m = (Z_n^m(-u,-v) - Z_n^m(0,0))\left(1+\frac{u^2+v^2}{(OA)(AR)}\right). \tag{20}$$

The γ_n^m terms are the weight functions found by combining Eqs. (3) and (4) to give

$$z_p = \sum_{n,m} c_n^m (Z_n^m(-u,-v) - Z_n^m(0,0))\left(1+\frac{u^2+v^2}{(OA)(AR)}\right) = \sum_{n,m} c_n^m \gamma_n^m. \tag{21}$$

The derivatives of γ_n^m required for Eqs. (18) and (19) are given by Eqs. (A10) and (A13) in Appendix A. If N image points are measured (indexed from e.g., $i=1,\ldots,N$), then Eqs. (16) and (17) yield $2N$ equations that reduce to matrix form $y=MC$, where

$$y = \begin{pmatrix} n_x(u_1,v_1) \\ n_y(u_1,v_1) \\ \vdots \\ n_x(u_N,v_N) \\ n_y(u_N,v_N) \end{pmatrix},$$

$$M = \begin{bmatrix} U_0(u_1,v_1) & U_1(u_1,v_1) & \cdots & U_{J-1}(u_1,v_1) \\ V_0(u_1,v_1) & V_1(u_1,v_1) & \cdots & V_{J-1}(u_1,v_1) \\ \vdots & \vdots & \ddots & \vdots \\ U_0(u_N,v_N) & U_1(u_N,v_N) & \cdots & U_{J-1}(u_N,v_N) \\ V_0(u_N,v_N) & V_1(u_N,v_N) & \cdots & V_{J-1}(u_N,v_N) \end{bmatrix},$$

$$C = \begin{pmatrix} c_0 \\ c_1 \\ \vdots \\ c_{J-1} \end{pmatrix}. \tag{22}$$

Each pair of rows in y and M corresponds to a single measured CCD point, while each column (of M) corresponds to a Zernike term indexed $j=0,\ldots,J-1$. The single index form[10] of the Zernike coefficients has been introduced for the sake of simplicity. These matrices are the same as those obtained in Eq. (30) of Ref. 8. The approach de-

scribed here is practically the same as that in Ref. 8, except those matrices were found by minimizing the residual of the error $e=y-MC$. In any case, the least-squares solution is given by [Eq. (31) of Ref. 8]

$$C=[M^TM]^{-1}[M^Ty], \tag{23}$$

where it will be assumed that the system contains many more rows than columns, and is therefore overdetermined. To summarize: (1) start with an initial c_n^m to give multiple estimates of $P=(x_p,y_p,z_p)$ for each measured point (u,v); (2) find (multiple) required normals n by Eqs. (11)–(13); (3) form U_n^m and V_n^m, given by Eqs. (18) and (19) for each point, and enter these into Eqs. (22) (along with n); and (4) solve for the new c_n^m using Eq. (23). Repeat from step (2) with the new c_n^m coefficients, until the method converges to a final solution. The convergence of this method has been demonstrated previously.[8,9] This standard method will be referred to as the recasted Sicam or the Sicam (RC) method.

B. Additional Step: Improving the Estimate of Corneal Sag

Equations (1)–(3) relate the corneal sag $F(-u,-v,z)$ to the intersection point $P(x_p,y_p,z_p)$ of a nearby ray. Figure 2 shows that these two points lie on the same (corneal) surface. In other words, the surface F defined by corneal sag coefficients c_n^m coincides (in theory) with the surface P described by the corneal intersection points (x_p,y_p,z_p). In practice, Eq. (3) involves several approximations, so that surfaces F and P will (in general) *deviate* from each other.

In fact, this predicted deviation has been plotted as the continuous lines (labeled "theory") shown in Figs. 3(a) and 3(b). These curves were determined by taking the corneal depth at the intersection point P, i.e., $z_p(x_p,y_p)$ as either spherical ($R=7$ mm) [Fig. 3(a)] or conical ($R=7.87$ mm, $p=0.82$) [Fig. 3(b)]. The deviation was calculated by using (x_p,y_p,z_p) in Eqs. (1) and (2) to give (u,v), from which $z(-u,-v)$ was obtained by Eq. (3). The difference $(z-z_p)$ has been plotted as a function of the common radial distance ρ.

The continuous deviation curves shown in Figs. 3(a) and 3(b) would be negligible if surfaces P and F coincided. Instead, these curves demonstrate an increasing error with radial distance. Because the Sicam (RC) method is based upon Eqs. (1)–(3), it is reasonable to ask whether this observation has implications for the reconstruction of the corneal sag. In fact, it will now be argued that the predicted deviations demonstrated in Figs. 3(a) and 3(b) will propagate to the coefficients generated by the Sicam (RC) algorithm. More specifically, it will be argued that these particular deviation curves model errors incurred by the Sicam (RC) algorithm, an observation that will be tested presently.

The Sicam (RC) algorithm finds a set of Zernike coefficients for the corneal sag F, that solve Eqs. (14) and (15). But these equations state that a normal to the surface P (rather than F) should bisect the incident and reflected ray [which is Eq. (11)] at a point (x_p,y_p,z_p). These conditions on P are the law of reflection, and characterize the corneal surface by hypothesis. It can be expected therefore [if Eqs. (14) and (15) are solved accurately] that surface P will more accurately represent the true corneal surface. Then the corneal sag surface $F(-u,-v,z)$ and hence the corneal sag z [described by Eq. (4)] is a *secondary* surface related only approximately to P by Eq. (3). This is, in fact, precisely the situation shown by the two theory curves in Fig. 3. These errors are calculated, assuming that $z_p(x_p,y_p)$ represents the true corneal surface (the sphere or conic surfaces tested in Fig. 3).

In summary, the algorithm as it has been described here will find coefficients c_n^m that determine the best intersection surface P (albeit indirectly), but the coefficients themselves correspond to F, which is an (error containing) estimate of the corneal sag. Fortunately, it is possible to circumvent these predicted errors. The corneal sag coefficients can be determined from the intersection (x_p,y_p,z_p) (i.e., surface P) directly. To demonstrate the point, additional steps are proposed, which enable a new and improved estimate of corneal sag to be made. These steps can be applied as an addition to the standard Sicam (RC) algorithm. Take the final c_n^m computed from the Sicam (RC) algorithm. Use these coefficients to calculate $z(-u,-v)$ by Eq. (4). Then use Eq. (3) to determine z_p, and Eqs. (1) and (2) to determine (x_p,y_p) for each of the N measured points. Compute a new estimate of corneal *sag*, realizing that z_p values are sags relative to points (x_p,y_p). In particular, form a least-squares system by using Eq. (23) with

$$y=\begin{pmatrix} z_p(u_1,v_1) \\ \vdots \\ z_p(u_N,v_N) \end{pmatrix},$$

$$M=\begin{bmatrix} Z_0(x_{p,1},y_{p,1}) & \cdots & Z_{J-1}(x_{p,1},y_{p,1}) \\ \vdots & \ddots & \vdots \\ Z_0(x_{p,N},y_{p,N}) & \cdots & Z_{J-1}(x_{p,N}+y_{p,N}) \end{bmatrix}, \quad C=\begin{pmatrix} \hat{c}_0 \\ \hat{c}_1 \\ \vdots \\ \hat{c}_{J-1} \end{pmatrix}, \tag{24}$$

thereby yielding new coefficients $\hat{c}_j \equiv \hat{c}_n^m$ corresponding to the improved corneal sag representation. As sag coefficients, they can be used in place of the original Sicam (RC) coefficients defined in Eq. (4) without further modification. The Sicam (RC) method with these additional steps will be referred to as the recasted and modified Sicam method, or the Sicam (RC+M) method, for the sake of brevity.

3. METHOD

A. Testing the Sicam (RC) and Sicam (RC+M) Methods

Simulations were conducted to contrast the Sicam (RC) and Sicam (RC+M) methods. Following the original Ref. 8 paper, a sphere ($R=7$, $p=1$) and a conic ($R=7.87$, $p=0.82$) were chosen for testing. A Zernike representation up to radial order 10 was selected and pupil diameter ($2a$) ranged from 7 up to 11 mm (taken in 1 mm steps). A toric surface tested the two methods in the nonsymmetric case. The toric had a central base radius of $R=7.8$ mm and modeled a large 7 D astigmatism along the vertical me-

ridian ($R_\perp = 6.71$ mm using a refractive index of 1.3375) [see Schwiegerling *et al.*[12] (1995) for calculation details].

The simulations required the positions of source points and their images as input to the reconstruction algorithm. Source points were determined as points corresponding to a circular grid (32×32) at the CCD plane, and were found by casting rays from the CCD grid points back through the (pinhole) camera to object space. The radius of the circular grid was chosen so the rays would fill the Zernike aperture of diameter $2a$ completely at the corneal surface. For the larger pupil sizes (e.g., 10 and 11 mm), it was found that peripheral rays were reflected in the direction of the positive z axis (i.e., to the right rather than reflecting in the direction of the camera). Therefore, source points were allowed to sit along the positive z axis (to the right of the cornea) if required. The nodal point was set to $OA = 300$ mm.

The Sicam (RC) and Sicam (RC+M) methods were applied using image and source points calculated at each particular pupil diameter. The methods started with a planar corneal shape, which was found to be a satisfactory starting point in all cases. The parameter AR was set to 7 mm for the sphere, 7.87 mm for the conic, and the mean of the principal radii of curvatures $AR = (7.8 + 6.71)/2 = 7.26$ mm for the toric. Testing of the toric showed the value of AR used did not affect the results appreciably. The absolute height errors were recorded along the corneal profiles for the three surfaces tested. In the case of the toric, results were recorded along the meridian of largest error (the vertical meridian).

B. Estimating Radius of Curvature R and p-Value p

The original Ref. 8 analysis used the sag coefficients to estimate central R and the conic p-value p for radially symmetric surfaces. Moreover, p was used to indicate efficacy of the reconstructed surface at the periphery. That is to say, a reconstruction of p close to the true value was used to indicate a good reconstruction. A large error in p was used to infer a breakdown in the algorithm.[8] The relationship between a given reconstruction method and estimates of R and p was investigated in more detail. The coefficients for the sphere and conic (obtained by the two methods used in Subsection 3.A) were entered into the equations

$$R = \frac{a^2}{2(2\sqrt{3}c_2^0 - 6\sqrt{5}c_4^0 + 12\sqrt{7}c_6^0 - 60c_8^0 + 30\sqrt{11}c_{10}^0)}, \tag{25}$$

$$p = \left(\frac{8R^3}{a^4}\right)(6\sqrt{5}c_4^0 - 30\sqrt{7}c_6^0 + 270c_8^0 - 210\sqrt{11}c_{10}^0), \tag{26}$$

derived for radial order 10 [errors in Eqs. (6) and (7) for radial order 6 in Ref. 8 are noted]. The *exact* least-squares coefficients were estimated up to radial order 10 and used in Eqs. (25) and (26) also. The formula

$$c_n^m = \frac{1}{\pi}\int_0^{2\pi}\int_0^1 z_a(a\rho,\theta)Z_n^m(\rho,\theta)\rho \mathrm{d}\rho \mathrm{d}\theta \tag{27}$$

was used, substituting z_a for the appropriate analytic solution (i.e., a sphere or conic). Adaptive Simpson quadrature was used with a 10^{-9} absolute tolerance. That produced very low absolute rms error, consistently less than residuals found using Sicam (RC) or Sicam (RC+M).

These coefficients estimated exact (in the least-squares sense and with low numerical error) coefficients bypassing the reconstruction process. Any deviation from true R and p estimated errors due to the finite Zernike representation (i.e., up to radial order 10). The R and p values varied depending on the method used, also indicating the differences between the Sicam (RC) and Sicam (RC+M) methods. An additional run was conducted for the sphere setting radial order to 14, thereby demonstrating the effect of increased radial order. All simulations were conducted using MATLAB (Mathworks, Natick, Virginia) and a MATLAB ray-tracing toolbox (RAYTRAK) developed by the author for simple ophthalmic applications.

4. RESULTS

A. Testing the Sicam (RC) and Sicam (RC+M) Methods

Figures 3(a) and 3(b) show log graphs of absolute height errors for spherical and conic corneas using the Sicam (RC) method. The distance from the corneal apex is shown along the horizontal axes, while absolute height errors are plotted on the vertical axes. The discrete data points are errors plotted for each pupil diameter setting, while the continuous curves show the theoretically predicted deviations (described in Subsection 2.B). In both figures, all reconstructed points were consistently submicrometer at distances less than ~3.5 mm from the corneal apex. However, as radial distance increased into the periphery, a significant error was observed. For example, data point errors at maximum radial distance ($\rho = 5.5$ mm) were 25.3 and 8.8 μm for the sphere and conic, respectively. The data points appeared to track the continuous theoretical deviation curves (as radial distance increased) in both cases.

Figure 4(a) and 4(b) show log error graphs of height errors for the sphere and conic using the Sicam (RC+M) method at each pupil diameter tested. These errors were consistently submicrometer, regardless of distance from the corneal apex. In fact, a significant (2 to 3 order of magnitude) drop [Fig. 4(a)] was observed for the sphere (errors ranged from $\sim 10^{-5}$ to $\sim 10^{-1}$ μm). In the case of the conic [Fig. 4(b)], a 3 to 4 order of magnitude drop was found (errors ranged from $\sim 10^{-6}$ to $\sim 10^{-2}$ μm).

Figures 5(a) and 5(b) show log error graphs for the Sicam (RC) and Sicam (RC+M) methods along the vertical meridian of the toric. This meridian was chosen because it contained the greatest reconstruction errors. For example, the maximum error in the vertical meridian error was 37 μm at the edge of the 11 mm pupil, against 11 μm for the horizontal meridian. The predicted deviations were included in Fig. 5(a) and again, the data points tracked along this theoretical curve as found for the sphere and conic. The maximum errors reduced to

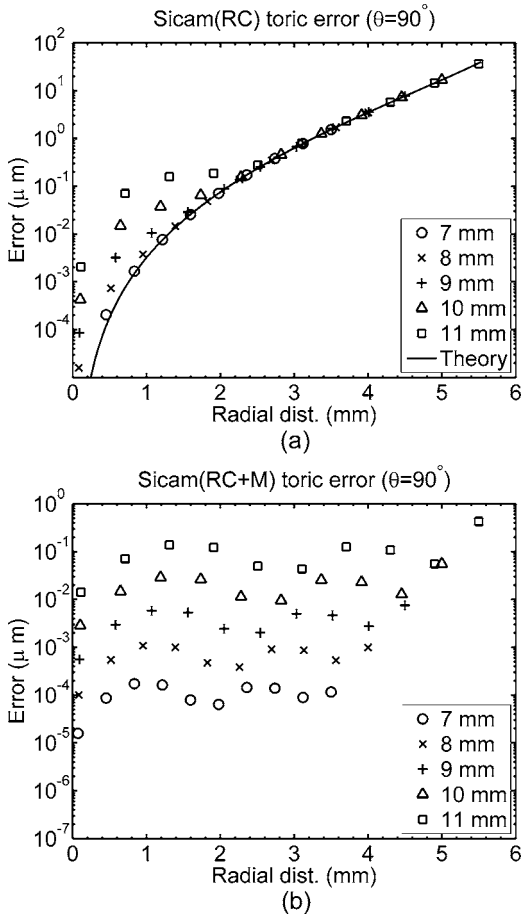

Fig. 5. Reconstruction results for a toric surface along the vertical meridian applied (a) using the Sicam (RC) method and (b) the Sicam (RC+M) method. The predicted deviation has been determined for the vertical meridian and is plotted as the continuous line in (a). Note the large reductions in error after the improved method has been applied.

$\sim$0.4 μm using the Sicam (RC+M) algorithm [Fig. 5(b)]. The toric error dropped 2 to 3 orders of magnitude along the vertical meridian, and the resultant error ranged from $\sim 10^{-5}$ to $\sim 10^{-1}$ μm.

In fact, this improvement is shown across the entire toric surface in Figs. 6(a) and 6(b). Figure 6(a) shows the complete error surface (at maximum pupil) using the Sicam (RC) algorithm. Figure 6(b) shows the improvement after the Sicam (RC+M) algorithm was applied. The marked improvement over the original method can be seen for all meridians. Interestingly, error lobes of height 0.4 μm caused a jump in error at the edge of the pupil. The errors just inside the pupil (away from the edge) dropped to 0.15 μm. This jump also appears in Fig. 5(b), which summarizes errors along the vertical meridian.

The improvements in adding the fitting step to the Sicam (RC) method were much larger than any errors incurred by the additional fitting to the raw (x_p, y_p, z_p) data. The mean absolute height errors due to the fitting were 3.2×10^{-3} μm, with a standard deviation of 6.5×10^{-3} μm across the three surfaces and multiple pupil diameters tested. The absolute height error in fitting was largest for the 11 mm pupil diameter, and did not exceed 2.1×10^{-2} μm.

B. Estimating Radius of Curvature R and Conic p-Value p

Tables 1 and 2 show R and p results for the sphere and the conic surfaces (using radial order 10). The data was formatted to be consistent with Tables 1 and 2 of Ref. 8. The columns summarize results found using the Sicam (RC), Sicam (RC+M), and exact methods. The estimates for R and p improved across columns (to the right), as might be expected. Similarly, and as observed in Ref. 8, errors increased as pupil diameter increased. The proportions of error incurred by a particular approach [relative to the total errors due to Sicam (RC)] were found to be relatively constant for any given pupil diameter (i.e., row of the table). For example, for Sicam (RC), the sphere (with maximum pupil diameter) produced errors of 17.0 μm and 0.145 (for R and p, respectively). The error in R was reduced by 14±1% using Sicam (RC+M), and 48±1% for the best method. For p, the error was reduced by 16±1% using Sicam (RC+M), and 44±0% using the best method. A much smaller reduction, but similar pattern of reductions was observed for the conic. At maximum pupil diameter the errors were 1 μm and 0.01 (for R and p, respectively). The reductions in the error of R were 18±1% using Sicam (RC+M) and 53±1% using the best method. The error in p was reduced by 20±1% [using Sicam (RC+M)] and 48±0% (the best method).

Table 3 shows results for the sphere at radial order 14, though only results for aperture diameters of 10 and

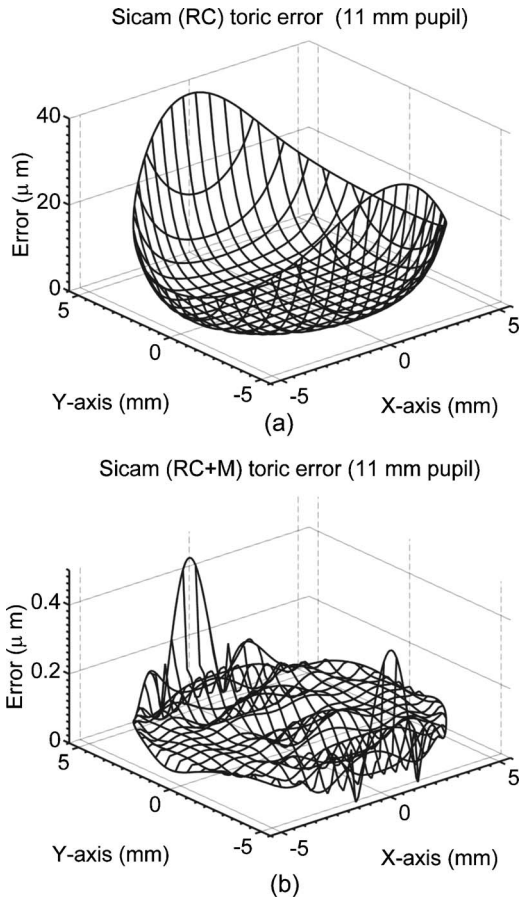

Fig. 6. Reconstruction results over the entire toric surface (a) using the Sicam (RC) method and (b) the Sicam (RC+M) method.

Table 1. Estimates of R and p for the Sphere (Radial Order 10)[a]

Pupil diameter (mm)	R (RC) (mm)	R (RC+M) (mm)	R (exact) (mm)	p (RC)	p (RC+M)	p (exact)
7	7.0000	7.0000	7.0000	0.999	0.999	0.999
8	6.9998	6.9998	6.9999	0.996	0.997	0.998
9	6.9990	6.9991	6.9995	0.987	0.989	0.993
10	6.9958	6.9964	6.9978	0.957	0.964	0.976
11	6.9830	6.9856	6.9909	0.855	0.880	0.918

[a]The Sicam (RC) columns estimate the original results presented in Ref. 8. The differences between the Sicam (RC) and Sicam (RC+M) columns estimate the impact of deviations in corneal shape due to reconstruction method. The exact columns deviate from true $R=7$ mm and $p=1$, as a result of the truncation of the finite Zernike representation.

Table 2. Estimates of R and p for the Conic (Radial Order 10)[a]

Pupil diameter (mm)	R (RC) (mm)	R (RC+M) (mm)	R (exact) (mm)	p (RC)	p (RC+M)	p (exact)
7	7.8700	7.8700	7.8700	0.820	0.820	0.820
8	7.8700	7.8700	7.8700	0.820	0.820	0.820
9	7.8699	7.8699	7.8700	0.819	0.819	0.819
10	7.8697	7.8697	7.8699	0.816	0.817	0.818
11	7.8690	7.8692	7.8695	0.810	0.812	0.815

[a]The Sicam (RC) columns estimate the original results presented in Ref. 8. The differences between the Sicam (RC) and Sicam (RC+M) columns estimate the impact of deviations in corneal shape due to reconstruction method. The exact columns deviate from true $R=7.87$ mm and $p=0.82$, as a result of the truncation of the finite Zernite representation.

Table 3. Estimates of R and p for the Sphere (Radial Order 14)[a]

Pupil diameter (mm)	R (RC) (mm)	R (RC+M) (mm)	R (exact) (mm)	p (RC)	p (RC+M)	p (exact)
10	6.9998	6.9999	6.9999	0.997	0.997	0.998
11	6.9988	6.9990	6.9994	0.981	0.985	0.990

[a]The table includes only the rows for 10 mm and 11 mm because errors were negligible otherwise. The results for the conic were not included because errors were completely negligible for all parameter values used.

11 mm are shown. Errors vanished (were negligible) for all lower aperture sizes. The errors that were observed were much smaller than the errors found for radial order 10. The conic information was not included for radial order of 14, because measured errors completely vanished over all R and p values tested.

5. DISCUSSION

A. Comparing the Sicam (RC) and Sicam (RC+M) Methods

The Sicam (RC) reconstruction results revealed errors that increased with radial distance. These errors were found to be significant (greater than submicrometer), particularly as distance extended into the periphery (>3.5 mm). These errors were suggested to arise as a result of the assumptions used to derive Eq. (3). The theory curves shown in Figs. 3(a), 3(b), and 5(a) predicted the expected deviation based on this idea. The reconstructed data was consistent with these error curves, and hence this idea. Additional steps were suggested to circumvent the radially increasing error incurred by Sicam (RC). The modified Sicam (RC+M) algorithm produced better estimates of corneal sag than the unmodified Sicam (RC) method across the surfaces and pupil diameters tested. The Sicam (RC+M) method reduced this height error by 2 to 4 orders of magnitude, to well below micrometer error in all cases. The results for the toric surface (with high 7 D astigmatism) indicated that skew rays could be dealt with by discrete points. These results are encouraging, and support further investigation of the discrete source approach to corneal reconstruction.

The errors for the Sicam (RC) algorithm appeared to enter through Eq. (3). An advantage of the new derivation was that sources of algorithm error were readily identifiable. These assumptions were: (i) the expansion to first order, (ii) the parabolic assumption, and (iii) the approximation $\Delta\rho' \approx \Delta\rho$. It is possible to estimate the errors in Sicam (RC) that arise through these assumptions. For the sake of concreteness, consider a point on a spherical cornea pupil sitting at $\rho=5.5$ mm. Consider first a first-order expansion of this *sphere* about the point $\rho=5.5$ mm. The estimate of z_p [Eq. (5)] being of first order, will contain an error on the order of $(\Delta\rho')^2$. The magnitude of that error can be determined by tracing a ray back from the nodal point through the point D ($\rho=5.5$ mm, $z=0$ mm) to the in-

tersection point P (ρ=5.55 mm, z_p=2.7343 mm). The difference in the radial positions of D and P gives an error estimate of $(\Delta\rho')^2=(0.05)^2\approx 2.5$ μm. The $\Delta\rho'\approx\Delta\rho$ assumption will introduce a similarly small error in estimated z_p, because the difference between the two is only 1 μm. In fact, setting the nodal point of the camera far from the corneal apex ensures that this remains low (e.g., OA=300 mm was here).

The introduction of the second assumption (parabolic slope) is the source of the largest error. Replace the spherical slope in the first-order expansion [Eq. (5)] with the parabolic slope given by Eq. (8). The final absolute height error in z_p [with a new estimated depth of 2.7083 mm found by Eq. (5)] is then 26.0 μm, which is much larger than the order of errors introduced by the other two assumptions. In fact, that absolute error can be related to the error measured using the Sicam (RC) algorithm. From Eq. (3) it can easily be shown that $\varepsilon_z=\varepsilon_p(1+\rho^2/(OA)(AR))^{-1}$, where ε_z is the error in sag, assuming z_p is known exactly [i.e., essentially the error incurred by Sicam (RC)], and ε_p is the *absolute* error in z_p, assuming z is known exactly. Using ε_p=26.0 μm (calculated above) gives ε_z=25.6 μm. This is exactly the theoretical error observed at ρ=5.5 mm [and shown in Fig. 3(a)], though it is probably more useful to assume that $\varepsilon_p\approx\varepsilon_z$ for OA large. In any case, this analysis shows that the parabolic assumption introduces a large error into the Sicam (RC) algorithm. If the cornea deviates from being parabolic, a significant error can be expected. Conversely, if the cornea is close to parabolic, there will be a close match between the Sicam (RC) and Sicam (RC+M) methods.

It is worthwhile emphasizing that the errors that arise from the Sicam (RC) algorithm are *inherent* to the method, and will not be reduced significantly by increasing radial order or sampling. Indeed, the low errors obtained for Sicam (RC+M) showed that radial order and sampling were more than adequate for good estimates of corneal sag. However, it would be useful to investigate the optimal relationship between sampling and radial order on reconstruction, and would be an avenue for further research. In addition, it is noted that there was little error incurred by implementing the additional fitting steps of the Sicam (RC+M) algorithm (mean absolute height error of 3.2×10^{-3} μm and a standard deviation of 6.5×10^{-3} μm).

The algorithm described here assumed that a measured image point could be associated with a source point. That correspondence cannot be made using continuous rings (e.g., Placido-disk-based topography), and so it may seem that it is unsuitable in that situation. Nonetheless, that particular problem can be dealt with by making relatively minor adjustments to the current method. Halstead *et al.* traced rays back to the Placido cone at each iteration (for the current corneal estimate), and then moved these rays to the nearest valid ring by adjusting the corneal normals.[9] Thus correspondences were enforced. This step could easily be implemented in the current algorithm, and would involve computing updated values for $S=(x_s,y_s,z_s)$ at each iteration by the method just described (i.e., locating the nearest ring). Then the algorithm would continue from the point of the algorithm where Eqs. (11)–(13) are applied to estimate the required n without additional modifications.

B. Skew Rays and the Sicam (RC+M) Algorithm: Radial Keratotomy

Reference 8 presented results for RK example, consisting of a band of corrugations added to a parabolic base (originally used by Rand *et al.*[13] using a spherical base). That model was given by

$$z=\frac{\rho^2}{2R}+g(\rho,\theta),$$

where

$$g(\rho,\theta)=\begin{cases}\varepsilon\sin(8\theta), & \rho\geqslant 2\text{ mm}\\ 2(\rho-1.5)\varepsilon\sin(8\theta), & 1.5<\rho<2\text{ mm}\\ 0, & \rho\leqslant 1.5\text{ mm}\end{cases}\quad(28)$$

represented a ring of corrugations with amplitude ε. The undulations produced a rapid variation in corneal tilt, testing the potential limitations of the algorithm to skew rays. Figure 7 shows results using Sicam (RC+M), adopting methods already described (see Subsection 3.A), and a 7 mm pupil aperture. The graph shows errors (at the outer edge of corneal corrugations) plotted against a meridional angle. The complete error profile (taken around the cornea) exhibited a fourfold symmetry, so only angles up to 90° needed to be plotted.

These graphs show an undulating error, with a peak error that drops as order is increased. In fact, for a twelfth-order Zernike, the peak error is of the order of 1 μm, while for order 16, the errors are consistently submicrometer. As order increases further, so do the error curves. However, the reduction is only within the same order of magnitude. In fact, the results obtained appear to agree with the original Ref. 8 paper, where a 0.2 μm dis-

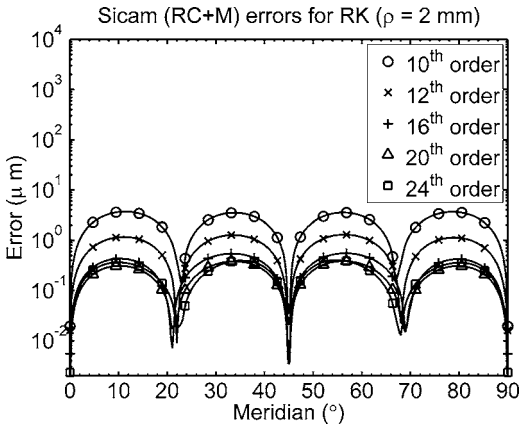

Fig. 7. Reconstruction results for the RK example showing errors as a function of meridian. Errors are shown at the outer edge (2 mm) of the band of corrugations for angles up to 90°. The resulting curves are consistently submicrometer for Zernike orders greater than or equal to 16. However, increasing the order beyond that limit gives relatively small reductions, *within* the order of magnitude (0.1 μm). For order 20, the results are similar to those presented in Ref. 8.

crepancy was observed at order 20. In turn, these results were consistent with results presented by Klein.[4,8]

The fact that error diminishes to below submicrometer error indicates that the algorithm can restore the corneal shape successfully. In other words, the information required for a good estimation is encoded (by discrete points) in the data. However, the order must be set high in order to extract that height from that data. That finding suggests a limitation of the present algorithm, particularly given that good estimations of a similar model were obtained previously using only low-order polynomials.[4,14] Indeed, it may be that there are representations (other than Zernike polynomials) that could capture the shape of abnormal corneas more efficiently. It may be that further improvements are possible, and would be an area for further research.

As mentioned, the results observed here are consistent with the results presented in Ref. 8, and hence the Sicam (RC+M) method produced similar results. That result is not entirely surprising. The base surface of the RK example tested (in Ref. 8) was a parabola. In that case, the assumption of a parabolic cornea [Eq. (6)] is satisfied. In Subsection 5.A, it was determined that as the cornea departs from being parabolic, a large error will be introduced into Eq. (3). With this assumption accounted for by the corneal model, the Sicam (RC) and Sicam (RC+M) methods will be very similar. The results shown here are therefore consistent with what might be expected.

C. Estimates of Radial Curvature R and p-Value p

The Sicam (RC) columns of Tables 1 and 2 are similar to those presented in Ref. 8 (see Tables 1 and 2 of that paper). This similarity suggests that the Sicam (RC) algorithm correctly synthesized the original Sicam *et al.* algorithm. In the Ref. 8 paper, the increasing errors in p (found as pupil diameter increased) were attributed to height errors incurred at the periphery of the cornea: in other words, a breakdown of the algorithm. In fact, the results suggest that the observed errors [in the Sicam (RC) column] were strongly influenced by the finite Zernike representation used (i.e., truncation of the Zernike sum). Indeed, increasing Zernike order (Table 3) virtually eliminated all of the observed errors in Table 1, showing that radial order rather than corneal height errors was the major cause of the observed errors. In fact, though it is not shown here, increasing radial error further would have reduced errors further still. The results for the conic at radial error 14 were not included because they were negligible over the entire set of parameters tested.

For radial order 10, the exact columns (Tables 1 and 2) showed that even a best estimate of the corneal profile could not match true p. These estimates showed that 56% (sphere) and 52% (conic) of the total error in p remained, even when using the exact reconstruction. The Zernike order prevented a further reduction in the error. The Sicam (RC) coefficients were found *after* the application of Eq. (3). The Sicam (RC+M) method gave coefficients found (in effect) *prior* to the application of Eq. (3). This difference estimates errors (in R and p) corresponding to the alternate height reconstructions [i.e., due to Eq. (3)]. Then, only a relatively modest proportion [i.e., roughly 16% (sphere) and 20% (conic)] of the total error actually corresponds to changes related to significant corneal shape differences. The remaining unaccounted 28% (sphere) and 28% (conic) of total error is the difference between the Sicam (RC+M) and the exact estimate. That is an estimate of the error incurred by the Sicam (RC+M) algorithm over and above the truncation error.

In any case, the points raised here indicate that conic p-value should be used cautiously. The values for both R and p depend critically on order (rather than height errors), and it is likely that only a modest proportion of observed error will correspond to differences due to corneal height errors. In light of the uncertainties alluded to above, it is perhaps an erudite decision to use more standard measures such as maximum and absolute height error or rms error, say as single-valued measures of algorithm efficacy.

6. FURTHER WORK

The improvements are encouraging, and show that discrete points can be used to recover symmetric–nonsymmetric surfaces accurately (at least in simulation). It would be useful to test the Sicam (RC+M) on more complicated corneal models (such as keratoconus), as well as real corneas. It would also be useful to investigate the effects of radial order, sampling, and alternative surface representations on recovery. The latter point raises the question as to whether there may be more efficient corneal representations that better describe abnormal corneas. Note that replacing the Zernike basis functions with some alternative in the Sicam (RC) step would not prevent coefficients from being obtained for clinical use. The Zernike polynomials could still be used at the fitting step implemented by Sicam (RC+M). Work is continuing on optimizing the Sicam (RC+M) algorithm.

APPENDIX A

Here we derive the equations that comprise the entries of Eq. (22). For simplicity consider only the equations with respect to the u parameter. The required equations for v follow by identical arguments. Consider then Eq. (14) and the tangent vector,

$$\frac{\partial P}{\partial u} = \frac{\partial}{\partial u}(x_p, y_p, z_p),$$

with respect to u. Evaluating the dot product in Eq. (14) gives

$$n_x \frac{\partial x_p}{\partial u} + n_y \frac{\partial y_p}{\partial u} - \frac{\partial z_p}{\partial u} = 0, \tag{A1}$$

where $n = (n_x, n_y, -1)$. Now, Eqs. (1) and (2) differentiate to give

$$\frac{\partial x_p}{\partial u} = -1 - \left(\frac{z_p}{OA}\right) - \left(\frac{u}{OA}\right)\frac{\partial z_p}{\partial u}, \tag{A2}$$

$$\frac{\partial y_p}{\partial u} = -\left(\frac{v}{OA}\right)\frac{\partial z_p}{\partial u}. \tag{A3}$$

Substituting Eqs. (A2) and (A3) into (A1) yields

$$n_x\left(1+\frac{z_p}{OA}\right)+\left(1+\frac{n_y v + n_x u}{OA}\right)\frac{\partial z_p}{\partial u}=0, \tag{A4}$$

after straightforward algebra. The z_p terms can be eliminated by using Eq. (21),

$$z_p = \sum_{n,m} c_n^m \gamma_n^m, \tag{A5}$$

where the identification

$$\gamma_n^m = (Z_n^m(-u,-v) - Z_n^m(0,0))\left(1+\frac{u^2+v^2}{(OA)(AR)}\right) \tag{A6}$$

was introduced. Taking the first derivative of z_p with respect to u gives

$$\frac{\partial z_p}{\partial u} = \sum c_n^m \frac{\partial \gamma_n^m}{\partial u}. \tag{A7}$$

Substituting Eqs. (A7) and (A5) into (A4) gives

$$n_x = \sum_{n,m} c_n^m U_n^m, \tag{A8}$$

where

$$U_n^m = -\left(1+\frac{n_y v + n_x u}{OA}\right)\frac{\partial \gamma_n^m}{\partial u} - \frac{n_x}{OA}\gamma_n^m, \tag{A9}$$

and

$$\frac{\partial \gamma_n^m}{\partial u} = \left(\frac{\partial Z_n^m(-u,-v)}{\partial u}\right)\left(1+\frac{u^2+v^2}{(OA)(AR)}\right) + (Z_n^m(-u,-v) - Z_n^m(0,0))\left(\frac{2u}{(OA)(AR)}\right). \tag{A10}$$

The first bracketed term of Eq. (A10) is the derivative of the 180° rotated Zernike polynomials with respect to u. Note also that Eq. (A6) and its derivative in Eq. (A10) can be precomputed since they have no dependence on n. Now the coefficients c_n^m in Eq. (A8) are the only unknowns. Then Eq. (A8) can be rearranged into matrix form, and in fact form the rows (in u) of entries in Eq. (22). Repeating identical arguments for the tangent vector,

$$\frac{\partial P}{\partial v} = \frac{\partial}{\partial v}(x_p, y_p, z_p)$$

gives

$$n_y = \sum c_n^m V_n^m, \tag{A11}$$

where

$$V_n^m = -\left(1+\frac{n_y v + n_x u}{OA}\right)\frac{\partial \gamma_n^m}{\partial v} - \frac{n_y}{OA}\gamma_n^m, \tag{A12}$$

and γ_n^m is again given by Eq. (A6). For completeness, the derivative with respect to v is

$$\frac{\partial \gamma_n^m}{\partial v} = \left(\frac{\partial Z_n^m(-u,-v)}{\partial v}\right)\left(1+\frac{u^2+v^2}{(OA)(AR)}\right) + (Z_n^m(-u,-v) - Z_n^m(0,0))\left(\frac{2v}{(OA)(AR)}\right). \tag{A13}$$

As with Eq. (A8) the equivalent equation in v [i.e., Eq. (A11)] can be rewritten in matrix form, which yields rows (in v) of the linear system of Eq. (22).

REFERENCES

1. S. E. Wilson, "Computerized corneal topography and its importance to wavefront technology," Cornea **20**, 441–454 (2001).
2. R. A. Applegate, "Noninvasive measurement of corneal topography," IEEE Eng. Med. Biol. Mag. **14**, 30–42 (1995).
3. S. A. Klein, "Axial curvature and the skew ray error in corneal topography," Optom. Vision Sci. **74**, 931–944 (1997).
4. S. A. Klein, "Corneal topography reconstruction algorithm that avoids the skew-ray ambiguity and the skew-ray error," Optom. Vision Sci. **74**, 945–962 (1997).
5. M. A. Halstead, B. A. Barsky, S. A. Klein, and R. B. Mandell, "A spline surface algorithm for reconstruction of corneal topography from a videokeratographic reflection pattern," Optom. Vision Sci. **72**, 821–827 (1995).
6. F. M. Vos, H. J. W. Spoelder, D. M. Germans, R. Hofman, and H. Bal, "Real-time, adaptive measurement of corneal shapes," Comput. Sci. Eng. **4**, 66–76 (2002).
7. F. M. Vos, R. G. L. van der Heijde, H. J. W. Spoelder, I. H. M. van Stokkum, and F. C. A. Groen, "A new instrument to measure the shape of the cornea based on pseudorandom color coding," IEEE Trans. Instrum. Meas. **46**, 794–797 (1997).
8. V. A. Sicam, J. Coppens, T. J. T. P. van der Berg, and R. G. L. van der Heijde, "Corneal surface reconstruction algorithm that uses Zernike polynomial representation," J. Opt. Soc. Am. A **21**, 1300–1306 (2004).
9. M. A. Halstead, B. A. Barsky, S. A. Klein, and R. B. Mandell, "Reconstructing curved surfaces from specular reflection patterns using spline surface fitting of normals," in *Proceedings of the Twenty-Third Annual Conference on Computer Graphics and Interactive Techniques* (ACM, 1996), pp. 335–342.
10. ANSI Z80.28-2004 Methods for reporting optical aberrations of the eye.
11. ISO 19980:2005 Ophthalmic instruments—corneal topographers.
12. J. Schwiegerling, J. E. Greivenkamp, and J. M. Miller, "Representation of videokeratoscopic height data with Zernike polynomials," J. Opt. Soc. Am. A **12**, 2105–2113 (1995).
13. R. H. Rand, H. C. Howland, and R. A. Applegate, "Mathematical model of a Placido disk keratometer and its implications for recovery of corneal topography," Optom. Vision Sci. **74**, 926–930 (1997).
14. J. Turuwhenua and J. Henderson, "A novel low-order method for recovery of the corneal shape," Optom. Vision Sci. **81**, 863–871 (2004).